REPORT DOCUMENTATION PAGE

Form Approved
OMB No. 0704-0188

1. AGENCY USE ONLY *(Leave blank)*	2. REPORT DATE	3. REPORT TYPE AND DATES COVERED
	March 1996	Professional Paper

4. TITLE AND SUBTITLE

CONFINED TWO-PHASE INCOMPRESSIBLE FLOWS

5. FUNDING NUMBERS

HPC Fellowship

6. AUTHOR(S)

T. S. Mautner

7. PERFORMING ORGANIZATION NAME(S) AND ADDRESS(ES)

Naval Command, Control and Ocean Surveillance Center (NCCOSC)
RDT&E Division
San Diego, CA 92152–5001

8. PERFORMING ORGANIZATION REPORT NUMBER

9. SPONSORING/MONITORING AGENCY NAME(S) AND ADDRESS(ES)

Naval Command, Control and Ocean Surveillance Center (NCCOSC)
RDT&E Division
San Diego, CA 92152–5001

10. SPONSORING/MONITORING AGENCY REPORT NUMBER

11. SUPPLEMENTARY NOTES

12a. DISTRIBUTION/AVAILABILITY STATEMENT

Approved for public release; distribution is unlimited.

12b. DISTRIBUTION CODE

13. ABSTRACT *(Maximum 200 words)*

This paper reportrs that the variable density, incompressible Navier-Stokes equations are solved using a technique based upon the Marker-and-Cell (MAC) method. The flow equations have been supplemented with the level set approach for interface tracking, and the required modifications to the MAC method are presented. This formulation has been used to solve several example problems, for closed containers, involving single and two-phase flows, various boundary conditions and several types of wall motion.

Published in *Proceedings of 26th AIAA Fluid Dynamics Conference*, Paper No. AIAA 95–2303, pp. 1–20, June 19, 1995.

14. SUBJECT TERMS

Mission Area: Command and Control (C^2)
Navier-Stokes Equations
Incompressible Flows
Marker-and-Cell (MAC) Method

15. NUMBER OF PAGES

16. PRICE CODE

17. SECURITY CLASSIFICATION OF REPORT	18. SECURITY CLASSIFICATION OF THIS PAGE	19. SECURITY CLASSIFICATION OF ABSTRACT	20. LIMITATION OF ABSTRACT
UNCLASSIFIED	UNCLASSIFIED	UNCLASSIFIED	SAME AS REPORT

21a. NAME OF RESPONSIBLE INDIVIDUAL	21b. TELEPHONE *(include Area Code)*	21c. OFFICE SYMBOL
T. S. Mautner	(619) 553–1621	Code 574

AIAA 95-2303
Confined Two-Phase Incompressible Flows

T. S. Mautner
NCCOSC RDTE Division
San Diego, CA

26th AIAA Fluid Dynamics Conference
June 19-22, 1995/San Diego, CA

Confined Two-Phase Incompressible Flows

T. S. Mautner
NCCOSC RDTE Division[1]
San Diego, CA 92152-6171

Abstract

The variable density, incompressible Navier-Stokes equations are solved using a technique based upon the Marker-and-Cell (MAC) method. The flow equations have been supplemented with the level set approach for interface tracking, and the required modifications to the MAC method are presented. This formulation has been used to solve several example problems, for closed containers, involving single and two-phase flows, various boundary conditions and several types of wall motion.

Introduction

A survey of recent literature indicates a strong interest in the computation of incompressible flows with density variations, free surfaces and bubbles rising and interacting with one another and with walls[1,6-10,12-15]. An integral part of these problems is the computation of the interface between the various fluid regions. In contrast to Lagrangian methods and the use of mass-less particles[2], various interface tracking and volume-of-fluid methods have been developed and provide an effective way to compute multi-phase flows (for examples, see Refs. 4-7, 9-11, 13-16).

Recently Osher and Sethian[11] introduced a "Hamilton-Jacobi" level set formulation of the equations for propagating interfaces. The level set approach implicitly captures the interface location, as the zero level of a smooth function, rather than explicitly tracking the front. With this method steep fluid gradients can be handled as well as the merging and breaking of fluid regions. The level set approach has been used to study fluid instabilities in compressible flows and incompressible flows with flame burning, shear layers, driven cavities and bubbles.

This paper applies the level set approach[11,13] to problems of fluids in closed containers with various forms of wall motion such as the driven cavity and translating container. The MAC method[2,3] has been extended to allow for variable fluid properties and surface tension. Results of the flow field and the interface motion will be presented along with estimates of the conservation of mass and stability requirements.

Nomenclature

D	divergence
F_R	Froude number = U/Lg
F_S	force due to surface tension
g	acceleration due to gravity
h	grid cell dimension - (Δx,Δy)
L	characteristic length
n	unit normal vector
p	pressure
Re	Reynolds number = UL/ν
t	time
Δt	time step
Δt_u	time step due to convection
Δt_ν	time step due to viscous terms
u	fluid velocity (u,v)
u_o	magnitude for translating box
u_{wall}	wall velocity
U	characteristic velocity
We	Weber number = ρU2L/σ
x,y	Cartesian coordinates
δ	delta function
ρ	fluid density
ρ_r	density ratio = ρ_2/ρ_1
ν	kinematic viscosity
μ	dynamic viscosity
μ_r	viscosity ratio = μ_2/μ_1
τ	viscous stress tensor
θ_{rot}	rotation angle
σ	surface tension coefficient
κ	curvature
ω	frequency
ω_o	over-relaxation parameter
α	interface thickness
ϕ	level set function
ϕ_o	level set function at previous time

[1]This paper is declared work of the U.S. Government and is not subject to copyright protection in the United States.

Governing Equations

The equations of motion are the variable density, incompressible Navier-Stokes equations[1]

$$\bar{\nabla}\cdot\bar{u}=0 \tag{1}$$

$$(\rho\bar{u})_t + \bar{\nabla}\cdot(\rho\bar{u}\bar{u}) = -\bar{\nabla}p + \bar{\nabla}\tau + \rho\bar{g} + \bar{F}_S \tag{2}$$

For immiscible liquids, the density and viscosity are constant along particle paths, thus they can be computed using

$$\rho_t + (\bar{u}\cdot\bar{\nabla})\rho = 0 \tag{3}$$

$$\mu_t + (\bar{u}\cdot\bar{\nabla})\mu = 0 \tag{4}$$

Using characteristic length, velocity, density and viscosity parameters, the non-dimensional form of the momentum equation is

$$(\rho\bar{u})_t = -\bar{\nabla}(\rho\bar{u}\bar{u}) - \frac{\rho\bar{g}}{F_R^2} + \left(-\bar{\nabla}p + \frac{1}{Re}\bar{\nabla}\cdot\tau + \bar{F}_S\right) \tag{5}$$

The Navier-Stokes equations are solved using a modified form of the SOLA[3] formulation of the MAC method of Harlow and Welch[2]. The method was modified to account for variable fluid properties, and the finite-difference expressions for the equations utilized the staggered MAC grid presented in Fig. 1. Even though this formulation is for constant density fluids, the pressure and density are considered separate terms instead of a single term, i.e. the kinematic pressure (p/ρ), as in the majority of incompressible models. Additionally, the viscosity is considered a variable in the viscous term formulation given by

$$\bar{\nabla}\cdot\tau = \mu\nabla^2\bar{u} + \bar{\nabla}\mu\cdot\bar{\nabla}\bar{u} \tag{6}$$

In general the velocities computed from Eqn (2) will not satisfy the continuity equation Eqn. (1). The SOLA method does not solve an elliptic equation for the pressure; however, the divergence free condition is obtained by adjusting the cell pressures. The pressures are determined iteratively, and the divergence D in each cell is computed using the most current values of the velocity components. The pressure change, Δp, required to make the divergence equal zero is

$$\Delta p = \frac{-\omega_o D}{2\Delta t\,\{(\Delta x)^{-2} + (\Delta y)^{-2}\}} \tag{7}$$

and the new pressure, at the k(th) iteration, is

$$p_{i,j}^{k+1} = p_{i,j}^{k} + \Delta p \tag{8}$$

The velocity components, at the cell faces, are adjusted to reflect the change in pressure using the following relationships

$$u_{i,j}^{k+1} = u_{i,j}^{k} + \frac{\Delta t}{\Delta x}\Delta p \tag{9}$$

$$u_{i-1,j}^{k+1} = u_{i-1,j}^{k} - \frac{\Delta t}{\Delta x}\Delta p \tag{10}$$

$$v_{i,j}^{k+1} = v_{i,j}^{k} + \frac{\Delta t}{\Delta y}\Delta p \tag{11}$$

$$v_{i,j-1}^{k+1} = v_{i,j-1}^{k} - \frac{\Delta t}{\Delta y}\Delta p \tag{12}$$

where the density is evaluated at the cell faces using, for example,

$$\rho_{i+1/2,j} = \frac{(\rho_{i,j} + \rho_{i+1,j})}{2} \tag{13}$$

Convergence of the pressure solution can be accelerated by multiplying Δp by an over-relaxation parameter, ω_o, where $1 \le \omega_o \le 2$.

Since the density and viscosity change sharply across an interface, conventional finite-difference techniques may not be able to handle the steep derivatives that would occur at these points. Thus, to capture the fluid interface, the level set technique[11,13] will be used. The level set function (ϕ) will be zero along the interface, positive in one fluid and negative in the other. The level set function is initialized as the signed normal distance to the interface and has the form

$$\phi_t + (\bar{u}\cdot\bar{\nabla})\phi = 0 \qquad (14)$$

This equation will transport the zero level set of ϕ exactly as the fluid interface moves. Also, since ϕ is a smooth function, it is more easily solved than Eqns. (3) and (4) for the density and viscosity. Now, in this formulation, the density and viscosity are defined by

$$\rho = \begin{cases} 1 & \text{if } \phi>0 \\ \rho_2/\rho_1 & \text{if } \phi<0 \\ (\rho_1+\rho_2)/\rho_2 & \text{if } \phi=0 \end{cases} \qquad (15)$$

$$\mu = \begin{cases} 1 & \text{if } \phi>0 \\ \mu_2/\mu_1 & \text{if } \phi<0 \\ (\mu_1+\mu_2)/\mu_2 & \text{if } \phi=0 \end{cases} \qquad (16)$$

The level set technique may develop jumps when interfaces interact, thus the level set function will be reinitialized to keep the distance function a distance function. First, to prevent instabilities at the interface, especially for large density/viscosity ratios, the density and viscosity can be smoothed according to

$$\bar{\rho} = (\rho_1+\rho_2)/2\rho_1 \quad \bar{\mu} = (\mu_1+\mu_2)/2\mu_1$$
$$\Delta\rho = (\rho_1-\rho_2)/2\rho_1 \quad \Delta\mu = (\mu_1-\mu_2)/2\mu_1$$

$$\rho(\phi) = \begin{cases} 1 & \text{if } \phi>0 \\ \rho_2/\rho_1 & \text{if } \phi<0 \\ \bar{\rho}+\Delta\rho\sin(\pi\phi/2\alpha) & \text{otherwise} \end{cases} \qquad (17)$$

and

$$\mu(\phi) = \begin{cases} 1 & \text{if } \phi>0 \\ \mu_2/\mu_1 & \text{if } \phi<0 \\ \bar{\mu}+\Delta\mu\sin(\pi\phi/2\alpha) & \text{otherwise} \end{cases} \qquad (18)$$

It should be noted that both the density and viscosity are smoothed across the interface region in contrast to Sussman et. al[13] who did not smooth the viscosity in this manner.

Reinitialization of the distance function is performed using the equation

$$\phi_t = S(\phi_o)\left\{1-\sqrt{\phi_x^2+\phi_y^2}\right\} \qquad (19)$$

where

$$S(\phi_o) = \frac{\phi_o}{\sqrt{\phi_o^2}} \qquad (20)$$

Applying the technique given by Sussman et. al.[13], the following expressions are used to solve Eqn. (19)

$$\begin{aligned} a&=(\phi_{i,j}-\phi_{i-1,j})/\Delta x \quad c=(\phi_{i,j}-\phi_{i,j-1})/\Delta y \\ b&=(\phi_{i+1,j}-\phi_{i,j})/\Delta x \quad d=(\phi_{i,j+1}-\phi_{i,j})/\Delta y \end{aligned} \qquad (21)$$

$$G(\phi) = \begin{cases} 0 & \text{if } \phi=0 \\ 1-\left(\max(b,0)^2+\min(a,0)^2\right. & \text{if } \phi<0 \\ \left.+\max(d,0)^2+\min(c,0)^2\right)^{1/2} & \\ 1-\left(\max(a,0)^2+\min(b,0)^2\right. & \text{if } \phi>0 \\ \left.+\max(c,0)^2+\min(d,0)^2\right)^{1/2} & \end{cases} \qquad (22)$$

Using these expressions, Eqn (19) now has the form

$$\phi^{k+1} = \phi^k + \Delta t\ S(\phi_o)\ G(\phi) \qquad (23)$$

and an iterative technique is used to drive the solution to steady state.

The surface tension term in Eqn (2) is

$$\bar{F}_s = \sigma\, \kappa\, \delta(d)\, \bar{n} \qquad (24)$$

and can be expressed in terms of the distance function as

$$\frac{1}{We}\, \kappa(\phi)\, \delta(\phi)\, \bar{\nabla}\phi \qquad (25)$$

where the curvature is

$$\kappa(\phi) = \bar{\nabla} \cdot \left\{ \frac{\bar{\nabla}\phi}{|\bar{\nabla}\phi|} \right\} \qquad (26)$$

and the delta function $\delta(\phi)$ can be approximated by

$$\delta(\phi) = \begin{cases} \frac{1}{2}\{1+\cos(\pi\phi/\alpha)\}/\alpha & |\phi|<\alpha \\ 0 & \text{other-wise} \end{cases} \qquad (27)$$

In smoothing the fluid properties and in the surface tension term, a reasonable value for the interface thickness is $\alpha \le 2\Delta x$. The examples in this paper were obtained using $\alpha=0$ and no surface tension effects were included.

The boundary conditions applied to the examples in this paper are both the no-slip and slip conditions at the solid walls. For the driven cavity problem, the top wall has a prescribed velocity of

$$u_{wall} \sin(\omega t) \qquad (28)$$

In the translating container case, an additional term was added to the x momentum equation to account for the coordinate translation. The term is

$$-\rho u_o \omega \sin(\omega t) \qquad (29)$$

and for container rotation, the gravity term becomes

$$\rho \theta_{rot} \sin(\omega t) \frac{\bar{g}}{F_R^2} \qquad (30)$$

Finally, at the solid walls, the level set function maintained a zero normal gradient. However, other boundary conditions could have been applied.

It is well known that the explicit formulations have time step limitations based upon the CFL condition for the convective terms, the viscous terms and the stiff source terms due to gravity and surface tension. The criteria used herein are based on the recommendations in Refs. 3, 6, and 13. For example, one can use

$$\Delta t_u \le \frac{\min}{\Omega} \left\{ \frac{\Delta x}{|u|}\ ,\ \frac{\Delta y}{|v|} \right\} \qquad (31)$$

and

$$\Delta t_v \le \frac{\min}{\Omega} \left\{ \text{const}\ \frac{\rho Re h^2}{\nu} \right\} \qquad (32)$$

then

$$\Delta t \le \min\left(\Delta t_u\ ,\ \Delta t_v\right) \qquad (33)$$

where the constant was suggested to be (3/14).[13] However, a value of approximately 0.043- 0.13 was used to obtain the time steps for the example cases. The time step data, obatained using Eqn. (32) exclusively, are shown in Table 1.

Finally, the solution algorithm can be summarized as follows:

Step 1. Initialize ϕ to be the signed normal distance to the interface.
Step 2. Initialize the fluid regions with the appropriate density and viscosity values.
Step 3. Compute the (u,v) velocity components using Eqns. (5)-(6).
Step 4. Compute the change in pressure to obtain a divergence free flow and update the (u,v) velocity components, Eqns. (7)-(12).
Step 5. Construct a new distance function by solving Eqn. (14) to steady state.
Step 6. Adjust the density and viscosity in the fluid regions, Eqns. (17)-(18).

Repeat steps 3-6 for each Δt.

Example Calculations

The computational method described above was applied to several problems involving confined flows. The results for a driven cavity, translating container, rotating container and a density driven flow will be given below. The input parameters are summarized in Table 1, and the arrangement of variables in a typical computational cell is shown in Figure 1. It should be noted that, in all computations, surface tension was not imposed, $g/(F_R)^2=1$, and the interface between the two fluid densities is located at the middle of the container at t=0.

1. Driven Cavity

The constant fluid property formulation of the method was tested using a driven cavity having from 5x5 to 200x200 rectangular grids. The results compared very favorably with, for example, SOLA[3] results. Figure 2 presents the velocity and pressure fields for a cavity with Re=1000 with a constant lid velocity, and the results agree well with computations made using a vorticity-stream function method.

The next case considered was the driven cavity having a sinusoidal lid velocity with frequency $\omega=0.63$ and Re=100. The frequency of oscillation produces two complete cycles in approximately t=20 non-dimensional time units. The results for the constant fluid property case are a given in Figs. 3 and 4 where the no-slip and slip boundary conditions were used. Both the velocity field and pressure contour data show the expected shift of the fluid's center of rotation due to the time-dependent lid velocity. At the points of maximum lid velocity, the results compare well with the uniform lid velocity case. Comparison of the data in Figs 3 and 4 shows the shift of the velocity's center of rotation with the change in boundary conditions.

Next, using a small density ratio, $\rho_r=0.9$, constant viscosity and $\omega=0.315$, the effect of grid density was examined. The results for the 50x50 grid are presented in Fig. 5 and the 100x100 grid results are given in Fig. 6. It is clear from the time histories of the interface location and the velocity field that the solution has not converged. Higher grid densities should be used to determine solution convergence. Another comparison, using the 100x100 grid, was made between the results obtained using the no-slip and slip boundary conditions. The results found in Figs. 6 and 7 once again show the differences in the computed results for the no-slip and slip boundary conditions. These differences are not unexpected and should remind one of the importance of using appropriate boundary conditions. The results also show that the level set formulation has no problem following the interface as it moves along the cavity wall and when it wraps up due to the rotating velocity field.

The final driven cavity example uses density and viscosity ratios of 0.5 and 0.2 respectively and a frequency $\omega=0.63$. The computed results are given in Fig. 8 and show that, with this higher density ratio, the velocity field has a large rotation confined to the lower density region (top) while a smaller velocity rotation occurs in the heavy fluid region (bottom). In this case the interface had only a small oscillatory motion. When one increases the density ratio to 10, the fluid motion is almost entirely confined to the lighter (top) fluid region with little or no interface motion. The $\rho_r=0.1$ results are not shown here.

2. Translating Container

The next case considered was that of a container, having a 2:1 aspect ratio, translating, sinusoidally in the horizontal direction, with frequency $\omega=0.63$ and magnitudes $u_o=1.0$ and 0.25, see Eqn. (29). Both cases used the same density ($\rho_r=0.5$) and viscosity ($\mu_r=0.2$) ratios, and the time histories of the interface motion and velocity fields are shown in Figs. 9 and 10. From the results of the higher magnitude of oscillation

case shown in Fig. 9 (u_o=1.0), the ability of the level set method to follow highly convoluted interface motion is clearly demonstrated. The interface contours look somewhat like that of a breaking wave. In contrast, the u_o=0.25 case shows a gentle sloshing of the fluid.

3. Rotating Container

Rotation of a rectangular container about its mid-point, aspect ratio of 4:1, was considered using the same density ratios as above but now considering a maximum rotation angle of 30 degrees with frequencies of rotation ω=0.315 and ω=0.628. The results of the interface motion and velocity field, over time, are plotted in Figs. 11 and 12. As before, the level set method follows the interface at all times and indicates a wave breaking like shape for the ω=0.315 case. The data in Fig. 12, ω=0.628, indicates that the flow has assumed a gentle sloshing pattern.

4. Density Driven Flow

The final example considered was a Rayleigh-Taylor instability problem. A density ratio of ρ_r=0.5 and a viscosity ratio of μ_r=0.2 were used where the heavy fluid was located in the upper half of the domain. The problem was started with the application of a small negative velocity (v=-0.25) along the middle 1/3 of the interface. The time evolution of the interface is given in Fig. 13 and shows the typical behavior found by many researchers. The slight asymmetric result is due to the uneven number of grid cells on each side of the mid-point along the interface. As in the many recent bubble computations, the interface moves smoothly along the wall at large times.

5. Interface Resolution

To illustrate the transition of fluid properties across the interface, selected portions of the interface from the rotating container at t=17 (Fig. 11) and the Rayleigh-Taylor problem at t=10 (Fig. 13) are shown in Fig. 14. It can be seen that for the "zero" interface thickness used in these examples, the density transitions over one grid cell with the zero of the level set function falling within. The interface locations and these density contours were obtained using the data computed at the cell centers shown in Fig. 1. If one plots interface and density contours using node point averaged data, the interface will be smeared over approximately 3 grid cells.

Stability and Conservation

Use of the stability criteria given in Eqns. (31)- (33) provided reasonable values for the time step in this explicit, finite-difference computation provided that the constant value in Eqn. (32) was reduced from 3/14[13] to approximately 0.043-0.13. The time step values given in Table 1 are conservative; however, the computation remained stable over long computation times. The computations also showed that the density and viscosity ratios play an important role in determining the appropriate time step. Also, an estimate of mass conservation (area in two dimensions) was made by simply counting the number of cell center points in the positive and negative regions of the level set function ϕ. The maximum error results are given in Table 1 and were determined from the maximum area ratios greater than and less than the nominal area ratio at t=0. It is encouraging that, even for the "zero" thickness interface, the maximum errors are less than 10% with the largest errors occurring during large distortions of the interface.

Conclusion

The computed results presented above indicate successful modification of the incompressible MAC/SOLA method to include variable density flows augmented with the level set approach for interface tracking. The finite-difference expressions followed the work of Daly[1] and Hirt et. al.[3] for the Navier-Stokes equations and a second order formulation for the level set method. The example problems demonstrated the ability of the method to track interface motion using a "zero" thickness interface (1 grid cell width) for density ratios up to 10. Higher density ratios could also be handled using some smoothing of the density and viscosity across the interface, for example Eqns. (17)-(18). The effects of grid density, wall motion and boundary conditions on the solution were also presented. Potential uses of this method could be the study of breaking waves and the transport of immiscible material.

Acknowledgments

This work was supported in part by this Center's High Performance Computing Fellowship Program and the Acoustic Analysis Branch (E. Rynne). Thanks go to Dan Park for his suggestions and discussions.

References

1. Daly, B., Numerical Study of Two Fluid Rayleigh-Taylor Instability, Phy. Fluids, Vol. 10, p. 297, 1967.

2. Harlow, F. and Welch, J., Incompressible Flows of Fluid with Free Surface, Phy. Fluids, Vol. 8, p. 2182, 1965.

3. Hirt, C., Nichols, B. and Romero, N., SOLA- A Numerical Solution Algorithm for Transient Fluid Flows, Report. No. LA-5852, Los Alamos Scientific Laboratory, 1975.

4. Hirt, C. and Nichols, B., Volume of Fluid (VOF) Method for the Dynamics of Free Boundaries, J. Comp. Physics, Vol. 39, p. 201, 1981.

5. Hyman, J., Numerical Methods for Tracking Interfaces, Physica, Vol. 12D, p. 396, 407.

6. Kothe, D., Mjolsness, R. and Torrey, M., RIPPLE: A Computer Program for Incompressible Flows with Free Surfaces, Report No. LA-12007-MS, Los Alamos National Lab., 1991.

7. Kothe, D. and Mjolsness, R., RIPPLE: A New Model for Incompressible Flows with Free Surfaces, AIAA J., Vol. 30, p. 2694, 1992.

8. Mansell, G., Walter, J. and Marschall, E., Liquid-Liquid Driven Cavity Flow, J. Comp. Physics, Vol. 110, p. 274, 1994.

9. Mulder, W. and Osher, S., Computing Interface Motion in Compressible Gas Dynamics, J. Comp. Physics, Vol. 100, p. 209, 1992.

10. Nobari, M. and Tryggvason, G., Numerical Simulations of Drop Collisions, Paper AIAA 94-0835, 32nd Aerospace Sciences Meeting, Reno, NV, Jan., 1994.

11. Osher, S. and Sethian, J., Fronts Propagating with Curvature-Dependent Speed: Alogorithms Based on Hamilton-Jacobi formulations, J. Comp. Physics, Vol. 79, p. 12, 1988.

12. Rouy, E. and Tourin, A., A Viscosity Solutions Approach to Shape-Form Shading, SIAM J. Numer. Anal., Vol. 29, p. 867, 1992.

13. Sussman, M., Smereka, P. and Osher, S., A Level Set Approach for Computing Solutions to Incompressible Two-Phase Flow, J. Comp. Physics, Vol. 114, 1994.

14. Szymczak, W., Rogers, J., Solomon, J. and Berger, A., A Numerical Algorithim for Hydrodynamic Free Boundary Problems, J. Comp. Physics, Vol. 106, p.319, 1993.

15. Unverdi, S. and Tryggvason, G., A Front-Tracking Method for Viscous, Incompressible, Multi-Fluid Flows, J. Comp. Physics, Vol. 100, p.25, 1992.

16. Zhu, J. and Sethian, J., Projection Methods Coupled to Level Set Interface Techniques, J. Comp. Physics, Vol. 102, p. 128, 1992.

Table 1. Input parameters and error estimates for example problems.

Example	Fig. No.	Grid Size h	ρ_r	μ_r	B. C.[1]	Δt	ω^2, θ_{rot} u_o, u_{wall}	% Max Error[3]
Driven Cavity	2	200x200 0.005	1.0	1.0	No-Slip	0.001	ω=0 u_{wall}=1.0	----------
Driven Cavity	3	50x50 0.02	1.0	1.0	No-Slip	0.005	ω=0.630 u_{wall}=1.0	----------
Driven Cavity	4	50x50 0.02	1.0	1.0	Slip	0.005	ω=0.630 u_{wall}=1.0	----------
Driven Cavity	5	50x50 0.02	0.9	1.0	No-Slip	0.005	ω=0.315 u_{wall}=1.0	6.62/2.30
Driven Cavity	6	100x100 0.01	0.9	1.0	No-Slip	0.001	ω=0.315 u_{wall}=1.0	7.96/0.19
Driven Cavity	7	100x100 0.01	0.9	1.0	Slip	0.001	ω=0.315 u_{wall}=1.0	2.55/2.71
Driven Cavity	8	50x50 0.02	0.5	0.2	No-Slip	0.005	ω=0.630 u_{wall}=1.0	1.54/0.86
Translating Container	9	100x50 0.02	0.5	0.2	No-Slip	0.005	ω=0.63 u_o=1.0	3.45/1.63
Translating Container	10	100x50 0.02	0.5	0.2	No-Slip	0.005	ω=0.63 u_o=0.25	0.96/0.77
Rotating Container	11	200x50 0.02	0.5	0.2	No-Slip	0.005	ω=0.315 θ_{rot}=30°	7.58/2.50
Rotating Container	12	200x50 0.02	0.5	0.2	No-Slip	0.005	ω=0.628 θ_{rot}=30°	0.77/0.38
Rayleigh-Taylor	13	100x200 0.01	0.5	0.2	Slip	0.001	----------	2.84/5.16

Notes: 1. B.C. - Boundary Condition
2. Frequency used in: a) Eqn(28) for Figs. 2-8, b) Eqn(29) for Figs. 9-10; c) Eqn.(30) for Figs. 11-12.
3. Max error refers to % greater/less than nominal area ratio for interface.

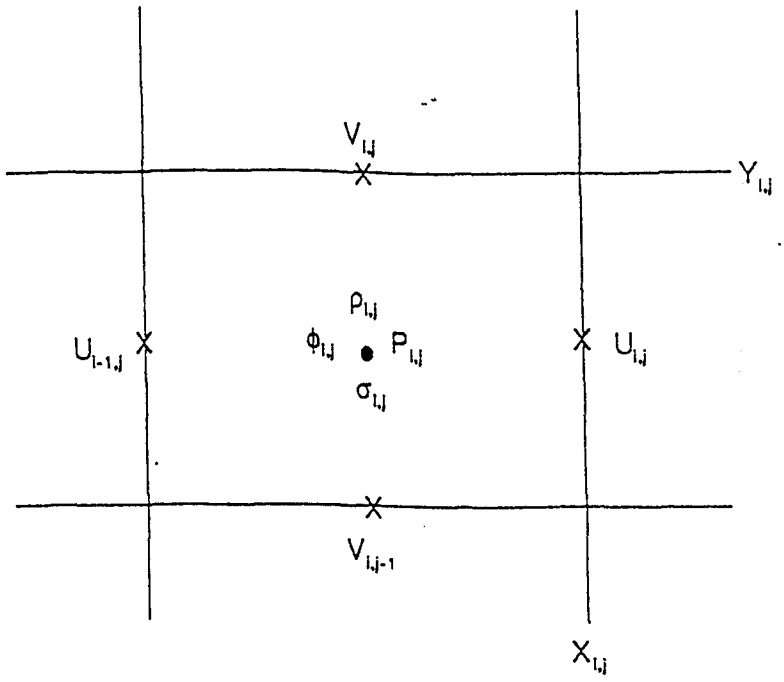

Figure 1. Arrangement of the variables in a typical computation cell.

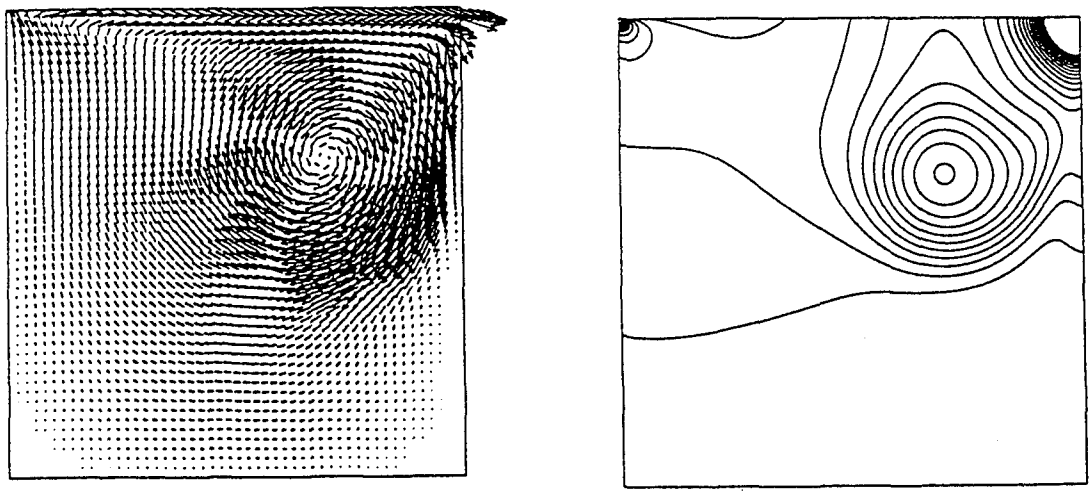

Figure 2. Velocity and pressure fields at t=4.9 for a driven cavity, Re=1000, no-slip boundary conditions and constant fluid properties.

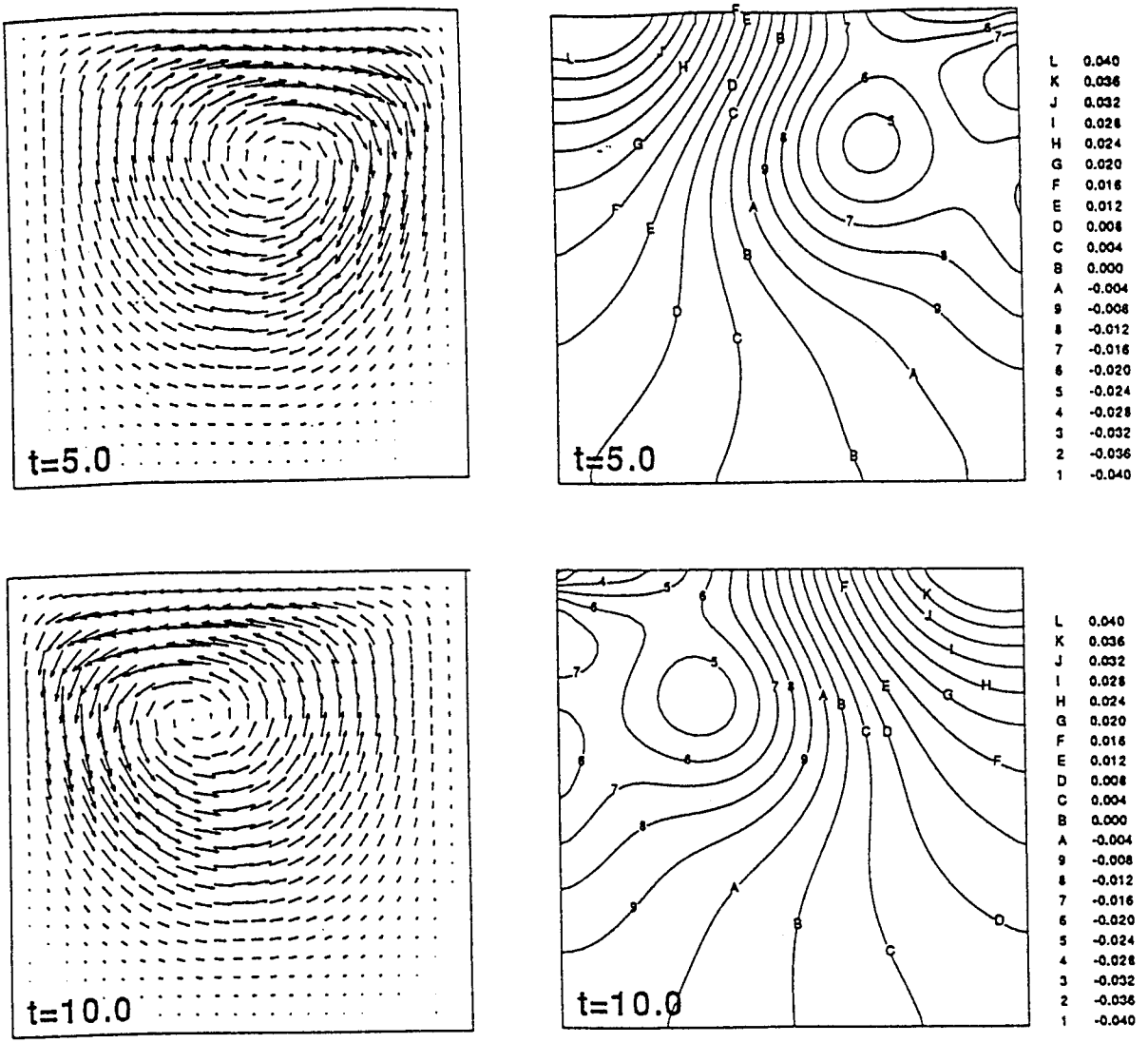

Figure 3. Velocity and pressure fields at t=5 and t=10 for a driven cavity, Re=100, no-slip boundary conditions and constant fluid properties.

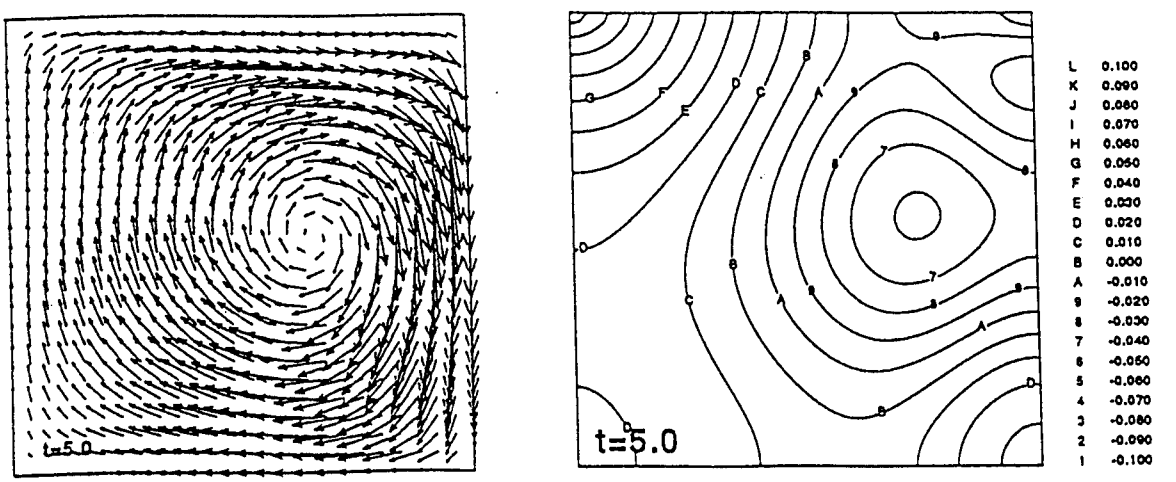

Figure 4. Velocity and pressure fields at t=5 for a driven cavity, Re=100, slip boundary conditions and constant fluid properties.

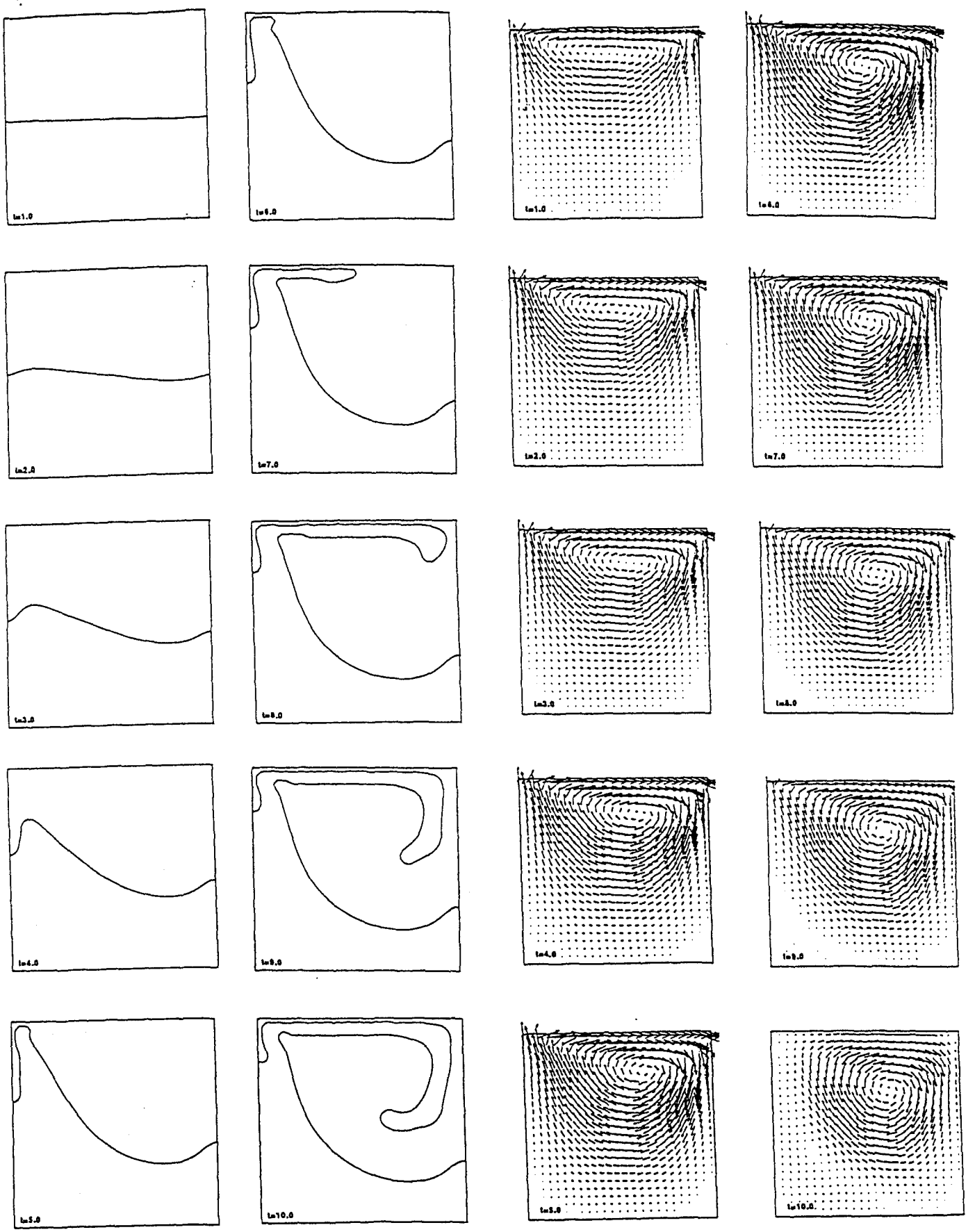

Figure 5. Interface location and velocity field for a driven cavity, Re=100, no-slip boundary conditions, ρ_r= 0.9, μ_r=1.0 and grid size of 50x50.

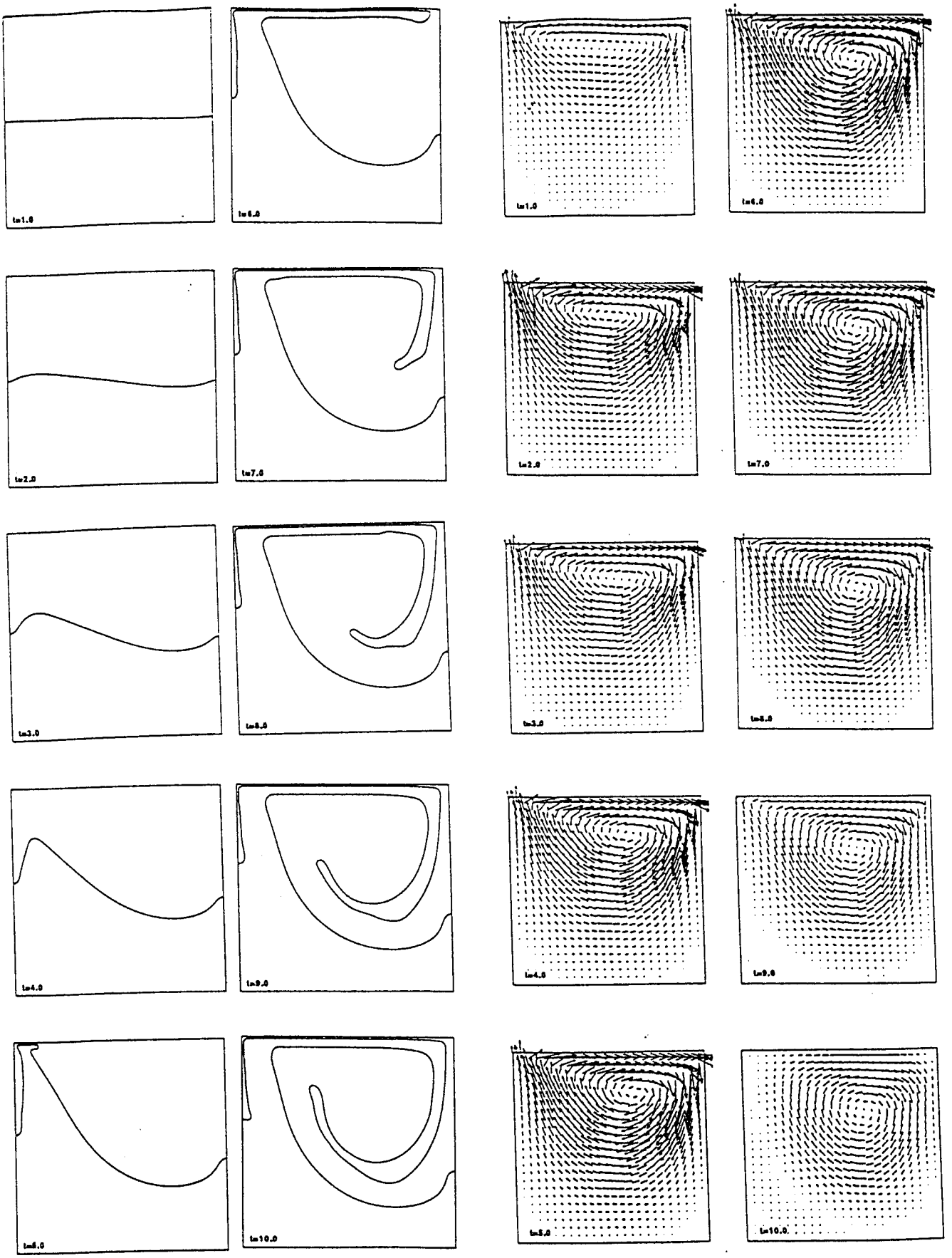

Figure 6. Interface location and velocity field for the driven cavity, Re=100, no-slip boundary conditions, ρ_r=0.9, μ_r=1.0 and grid size of 100x100.

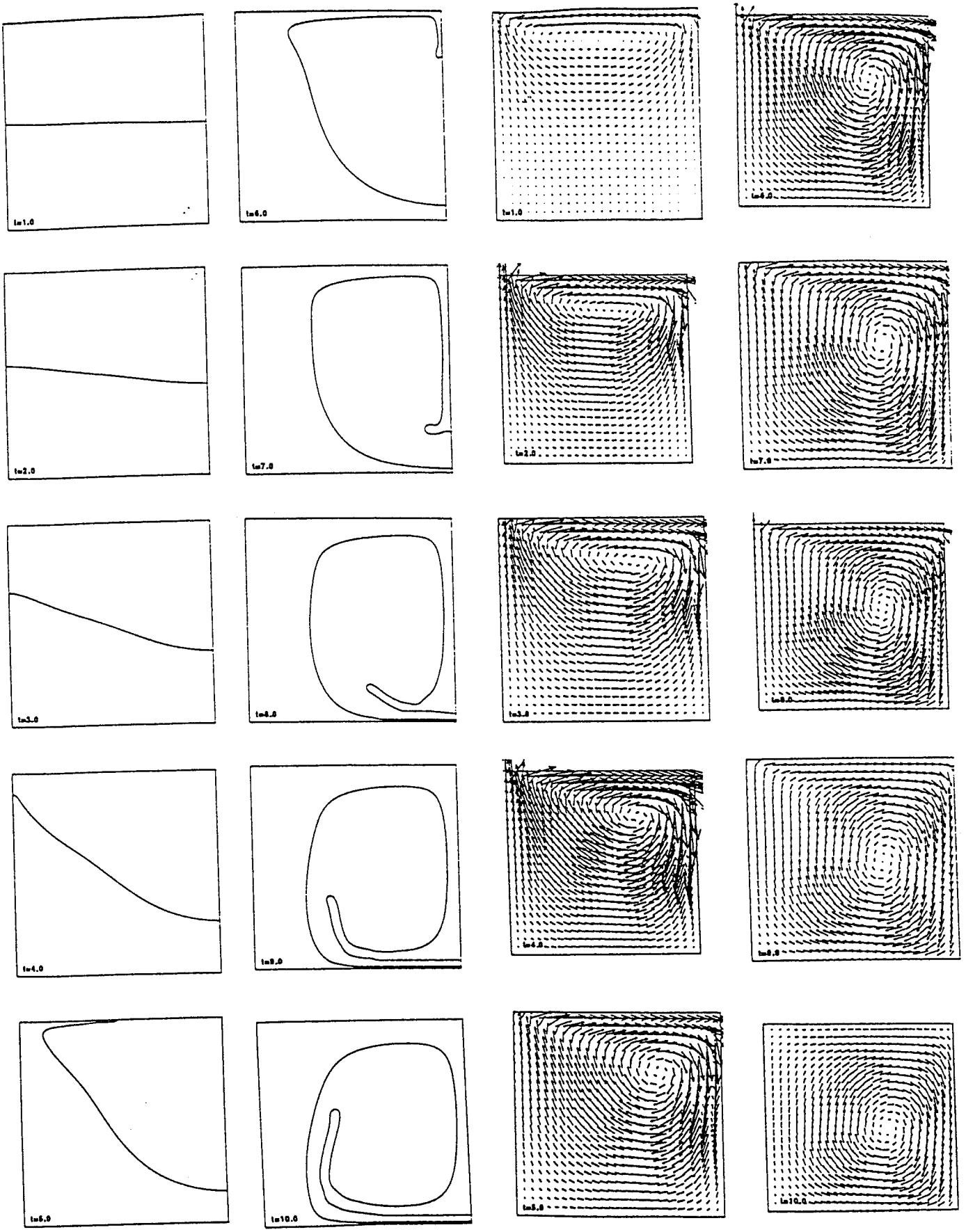

Figure 7. Interface location and velocity field for the driven cavity, Re=100, slip boundary conditions, ρ_r=0.9, μ_r=1.0 and grid size of 100x100.

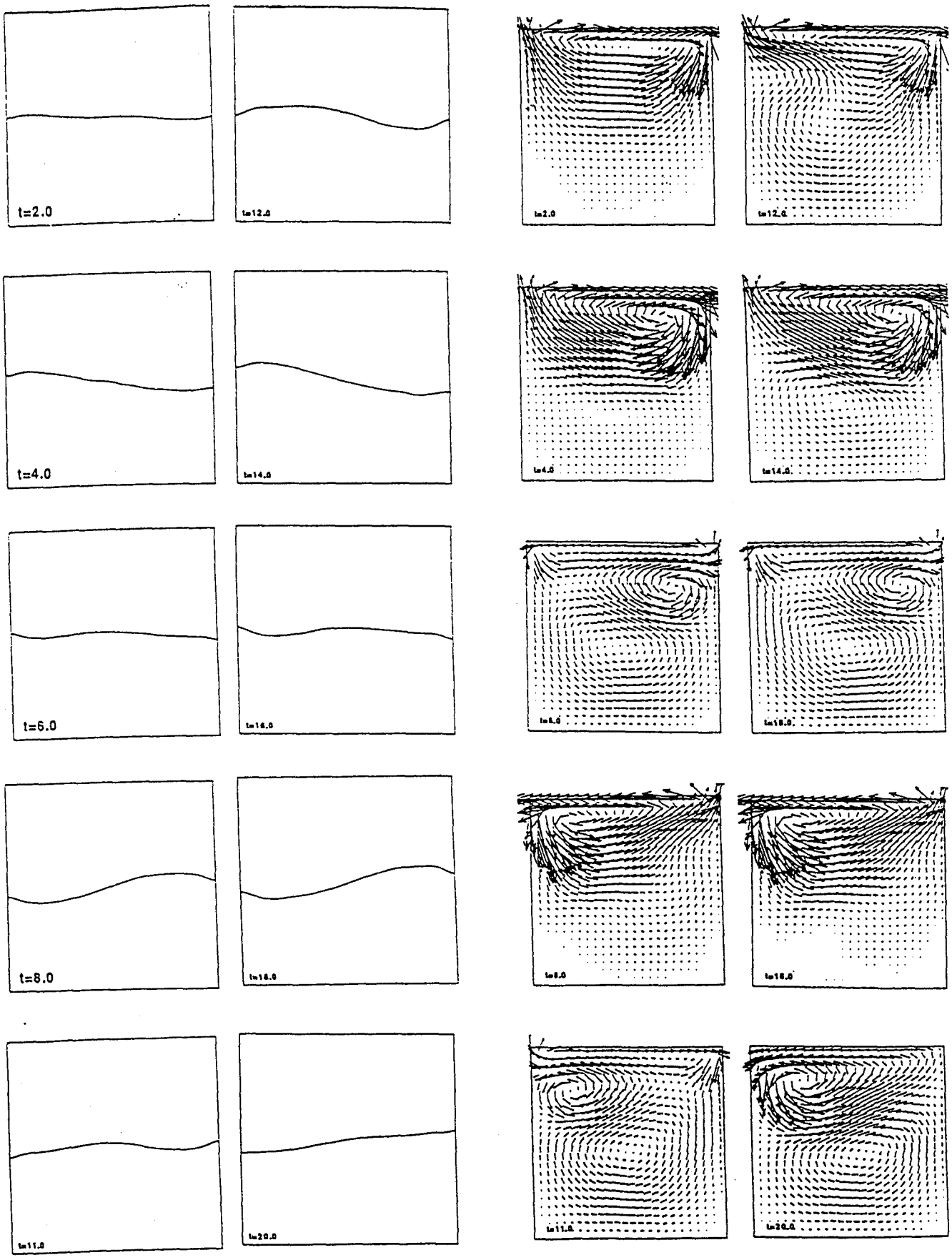

Figure 8. Interface location and velocity field for the driven cavity, Re=100, no-slip boundary conditions, ρ_r=0.5, μ_r=0.2 and grid size of 50x50.

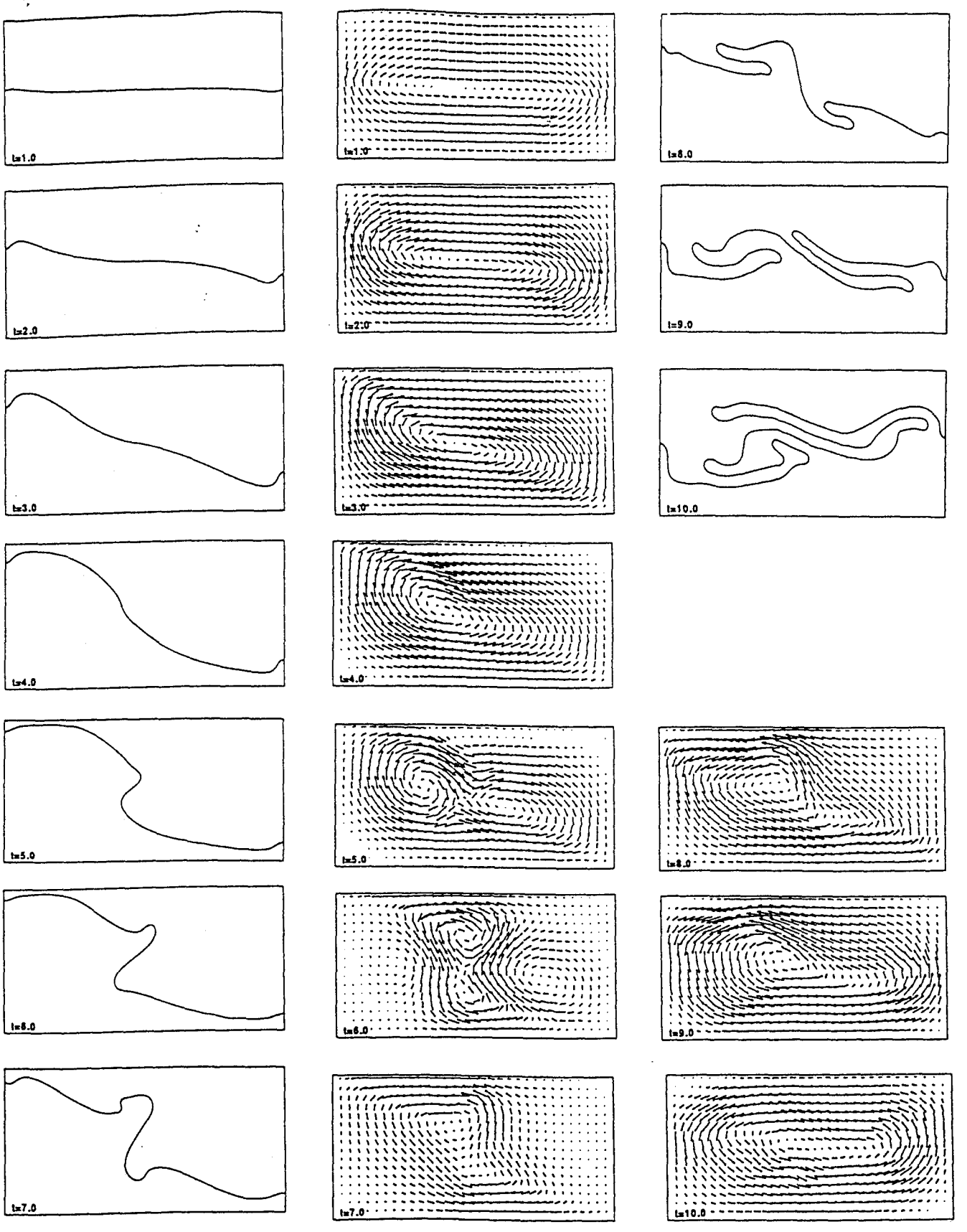

Figure 9. Interface location and velocity field for a translating box, Re=100, u_o=1.0, ρ_r=0.5 and μ_r=0.2.

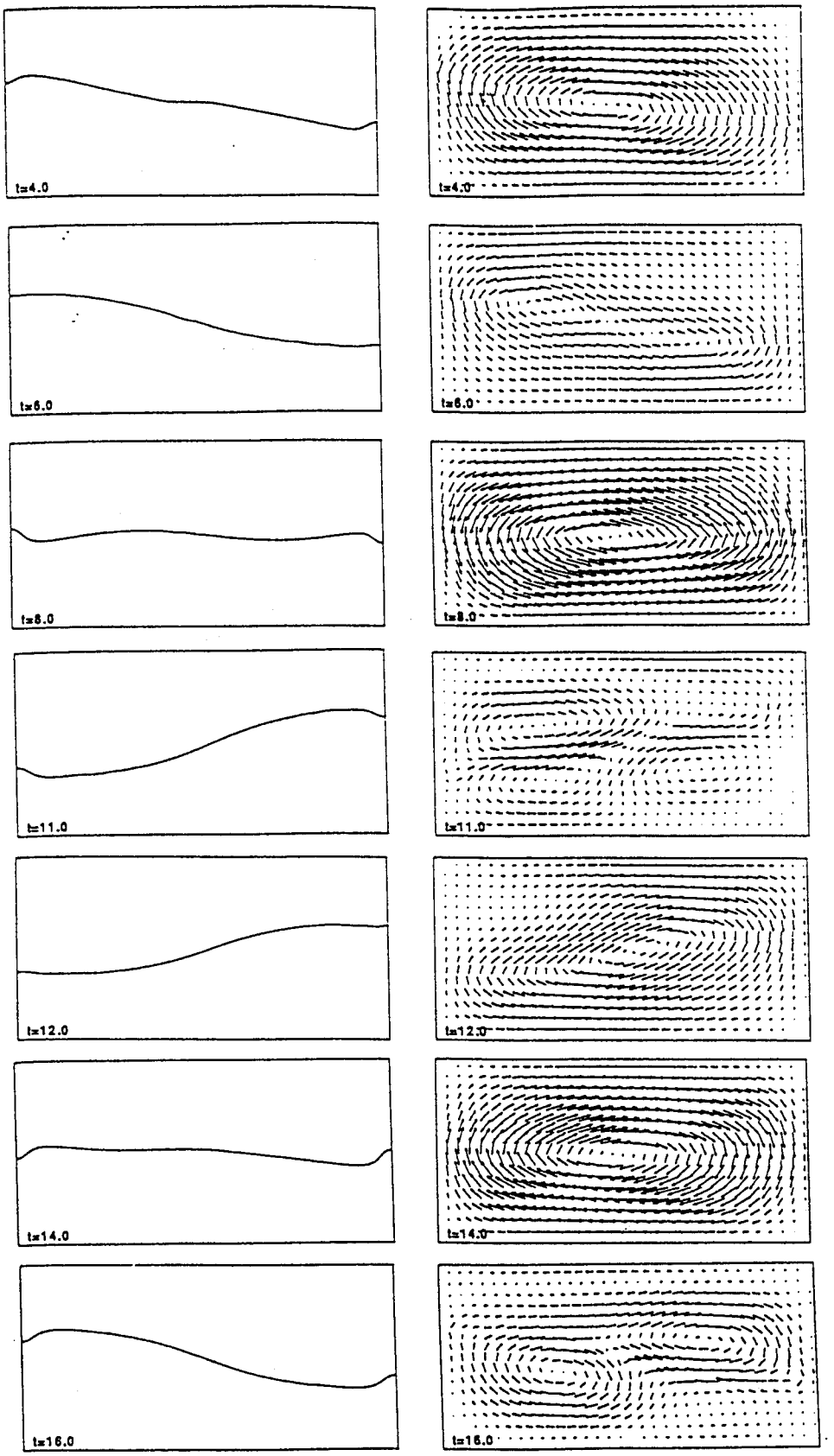

Figure 10. Interface location and velocity field for a translating box, Re=100, u_o=0.25, ρ_r=0.5 and μ_r=0.2.

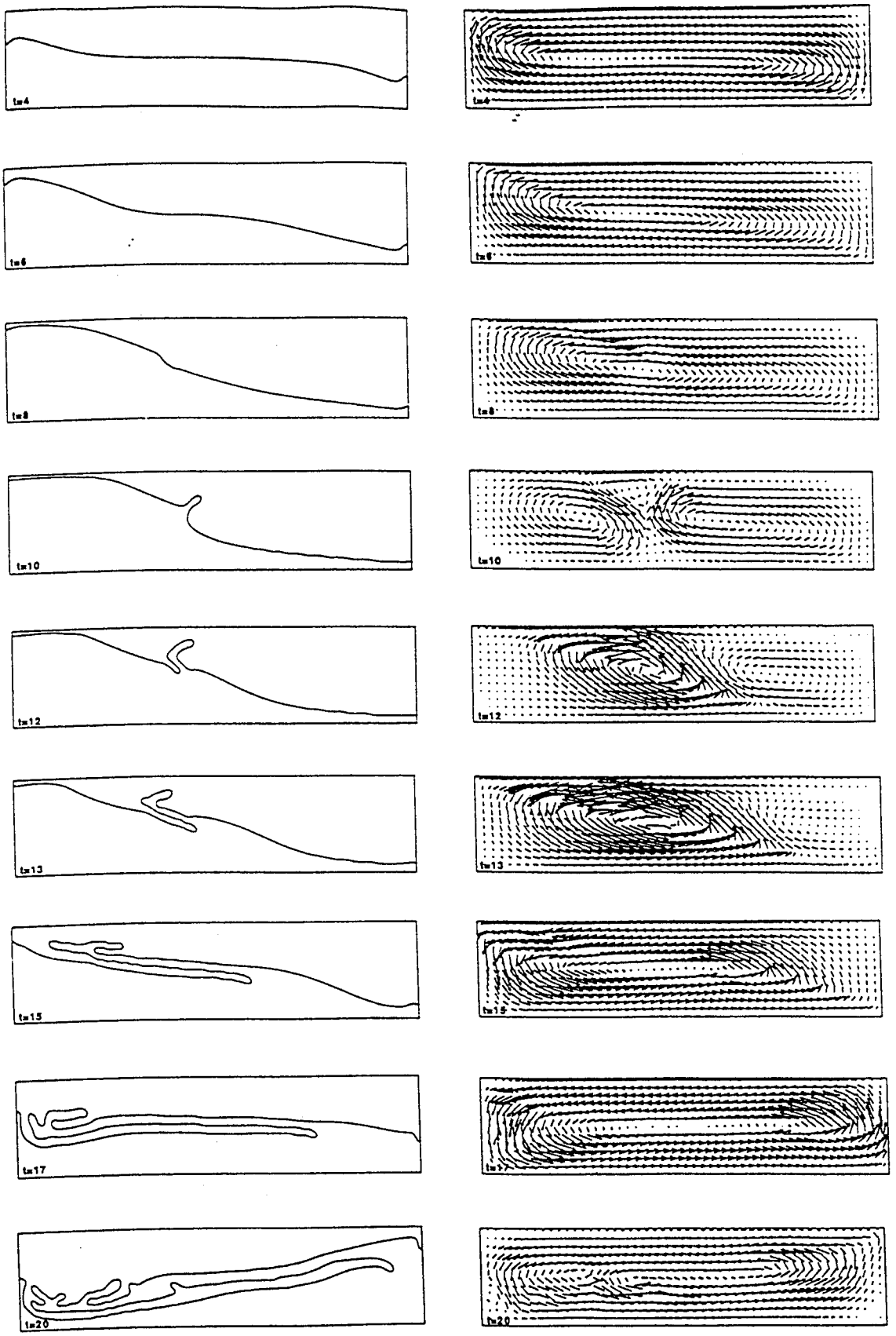

Figure 11. Interface location and velocity filed for a rotating box, Re=100, θ_{rot}=30*sin(0.315·t), ρ_r=0.5 and μ_r=0.2.

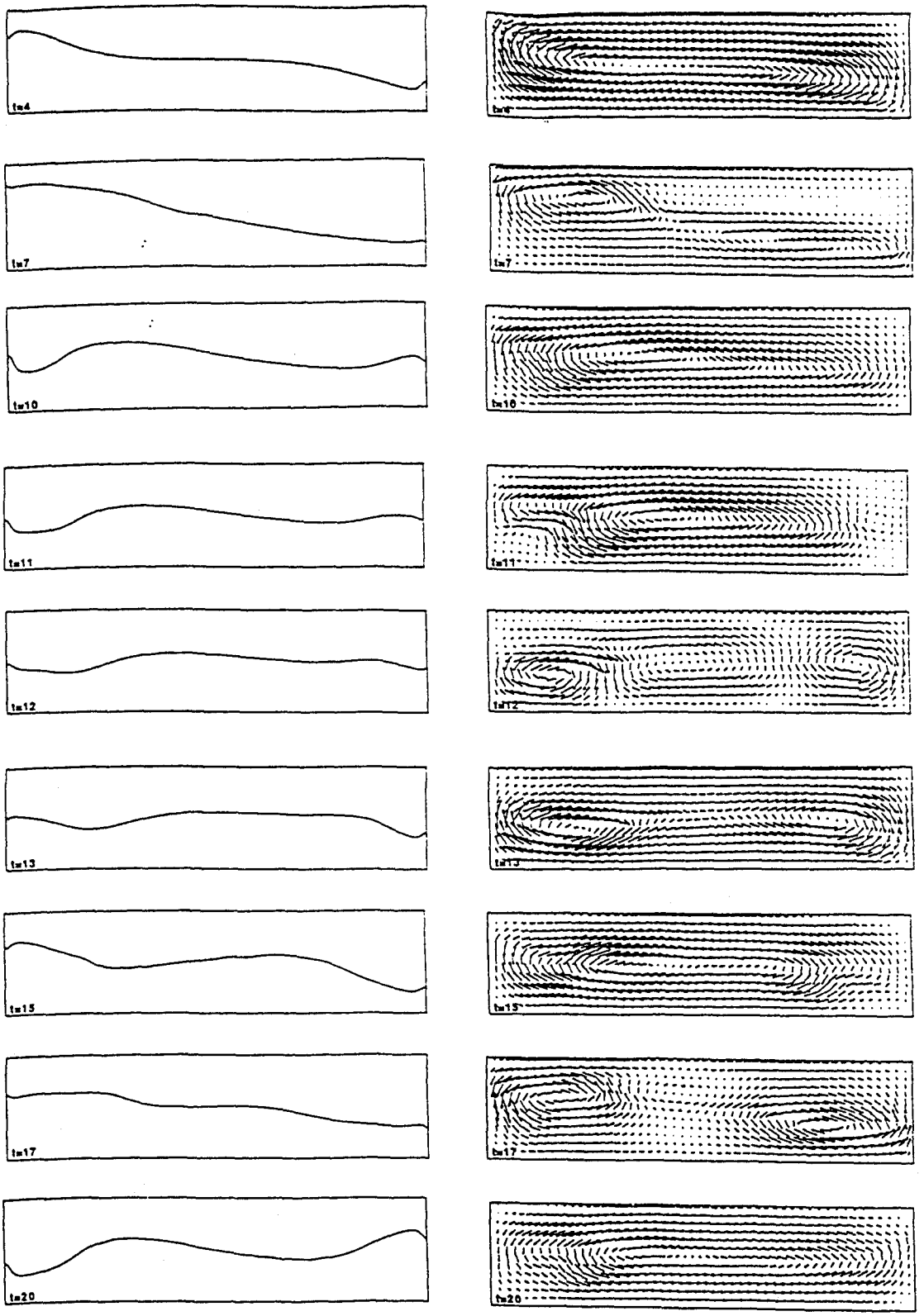

Figure 12. Interface location and velocity filed for a rotating box, Re=100, θ_{rot}=30*sin(0.628·t), ρ_r=0.5 and μ_r=0.2.

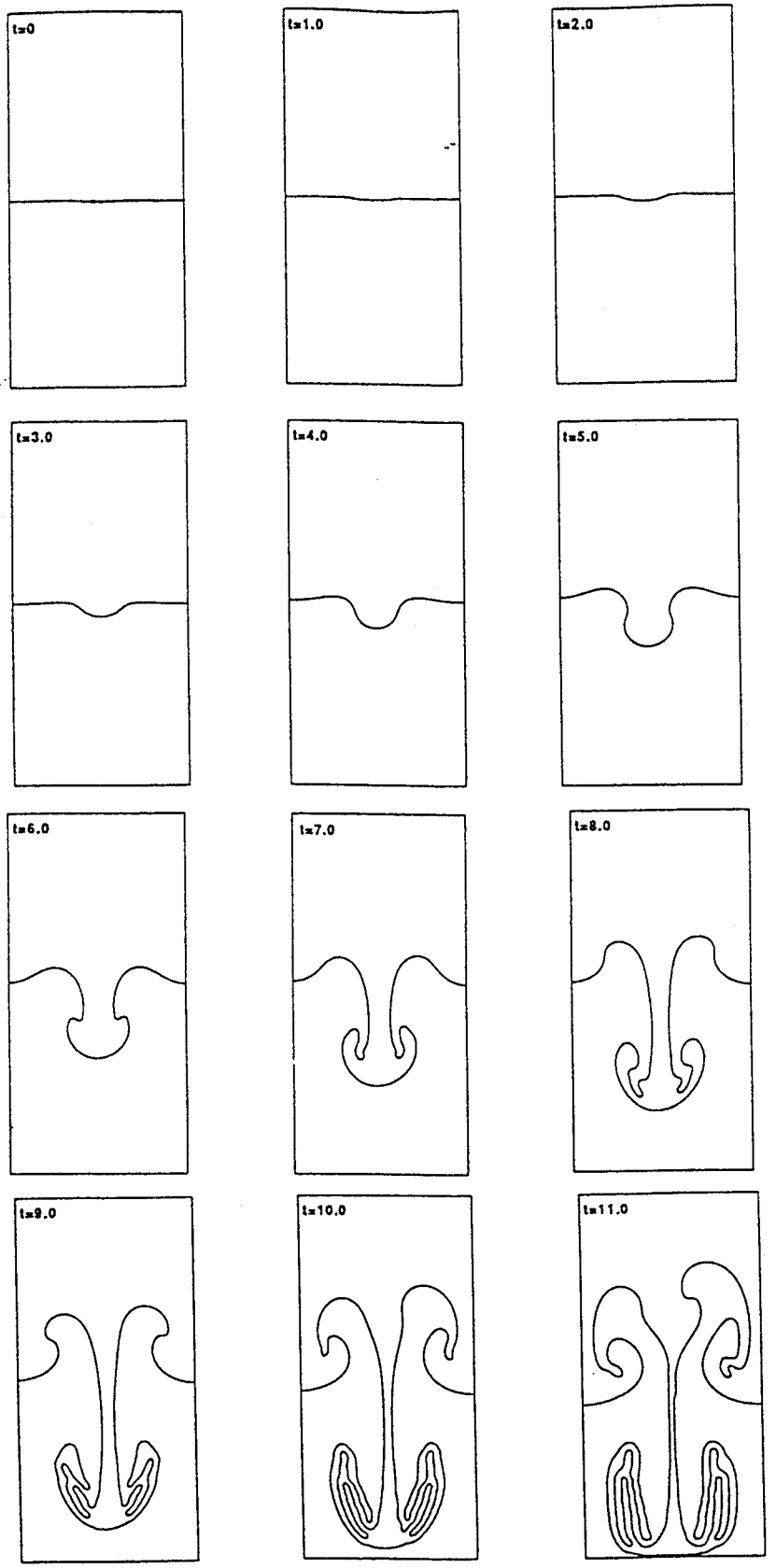

Figure 13. Interface location for a two fluid Rayleigh-Taylor instability, ρ_r=0.5 and μ_r=0.2.

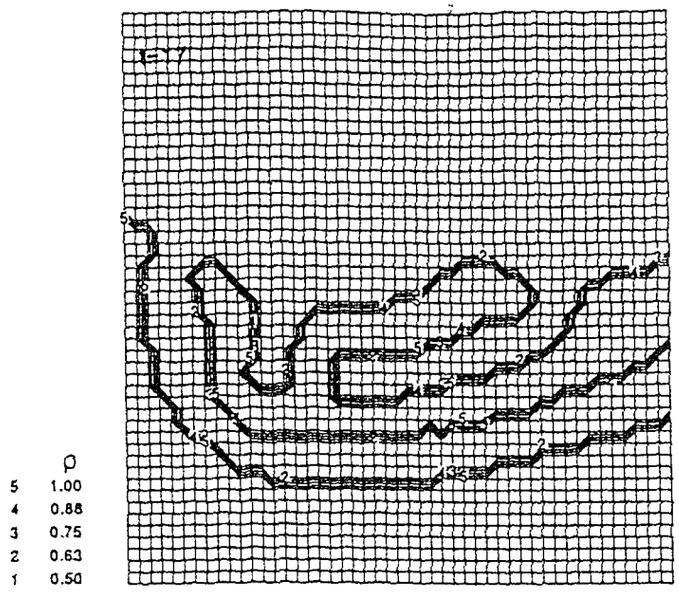

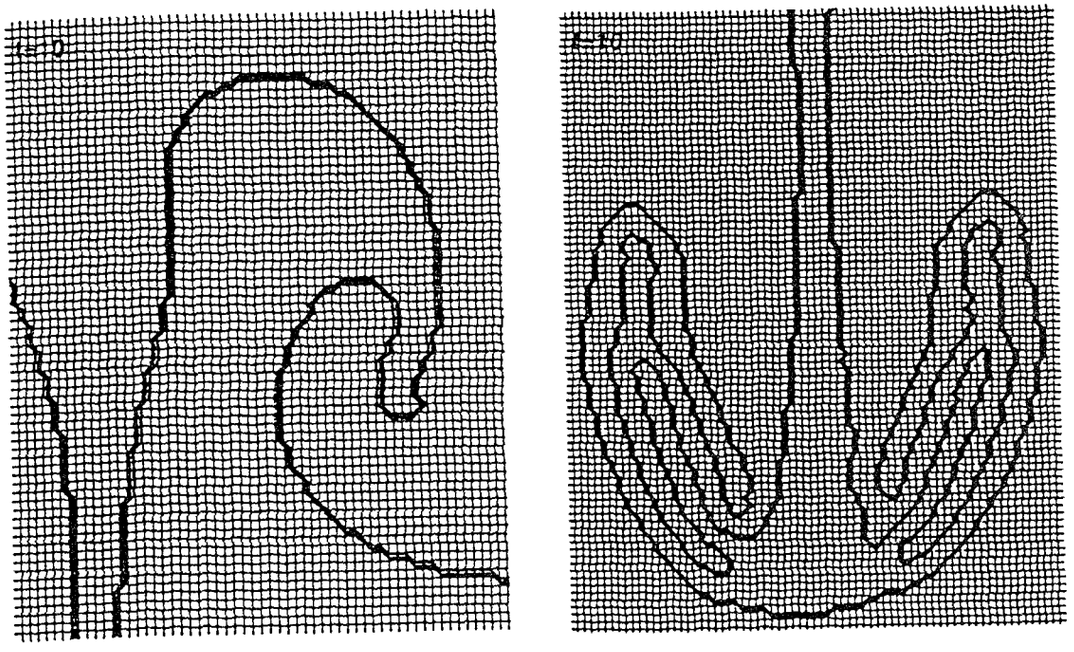

Figure 14. Examples of density interface contours for the rotating container and the Rayleigh-Taylor examples.